Molecular Crystals and Liquid Crystals

Publication details, including instructions for authors and subscription information:
http://www.tandfonline.com/loi/gmcl20

MODELLING MULTI-DIMENSIONAL OPTICS IN COMPLEX LIQUID CRYSTAL STRUCTURES AND DISPLAYS

Emmanouil E. Kriezis [a] & Steve J. Elston [a]

[a] University of Oxford, Department of Engineering Science, Oxford OX1 3PJ, United Kingdom

Version of record first published: 15 Jul 2010

To cite this article: Emmanouil E. Kriezis & Steve J. Elston (2003): MODELLING MULTI-DIMENSIONAL OPTICS IN COMPLEX LIQUID CRYSTAL STRUCTURES AND DISPLAYS, Molecular Crystals and Liquid Crystals, 401:1, 75-85

To link to this article: http://dx.doi.org/10.1080/744815193

Mol. Cryst. Liq. Cryst., Vol. 401, pp. 75/[189]–85/[199], 2003

ISSN: 1542-1406 print/1563-5287 online
DOI: 10.1080/15421400390243192

Taylor & Francis
Taylor & Francis Group

MODELLING MULTI-DIMENSIONAL OPTICS IN COMPLEX LIQUID CRYSTAL STRUCTURES AND DISPLAYS

Emmanouil E. Kriezis and Steve J. Elston
University of Oxford, Department of Engineering Science, Oxford OX1 3PJ, United Kingdom

Finite Difference Time Domain (FDTD) numerical modelling of light scattering from complex structures in liquid crystals is undertaken. As an example, typical Polymer Dispersed Liquid Crystal (PDLC) configurations such as the radial, axial, bipolar and concentric structures are analysed. Two-dimensional studies are used together with Gaussian Beam illumination conditions. In addition, the scattering at the edge of an isolated twisted nematic pixel in a reflective device is modelled. Apart from the numerical discretisation, no other approximations are introduced.

Keywords: light scattering; polymer dispersed liquid crystals; twisted nematic; FDTD method

INTRODUCTION

The modelling of the interaction of light with complex structures in liquid crystals is of key importance in the understanding of advanced liquid crystal systems. For example, a dispersion of liquid crystalline substances into a solid polymeric material forms the basis of a class of materials referred to as Polymer Dispersed Liquid Crystals (PDLC). These materials are characterised by interesting electro-optical properties based on their inherent light scattering, and they find several applications in switchable window films, projections systems, flat panel displays and light shutters [1,2]. The key point for understanding their optical properties is the modelling of light wave interaction between the impinging wave and the complex liquid crystal director structure. In addition to such intrinsically complex structures, significant light scattering can take place at the vicinity of pixel edges in twisted nematic displays due to the rapid LC reorientation

EEK acknowledges the financial support of the EPSRC and the Royal Society. Helpful discussions with Dr. P. Torok are also acknowledged.

and this can substantially influence the contrast or other important display device parameters.

Theoretical light scattering studies of PDLC structures are mainly conducted by employing classical electromagnetic wave scattering techniques, under certain restrictive approximations. The simplest one is the Rayleigh approximation, which neglects phase shifts originating from different areas of the scattering object, and is thus applicable only to extremely small objects with radius $R < 50\,\text{nm}$ [2]. An enhancement is provided by the Rayleigh-Gans approximation, which although allowing for internal phase shifts, assumes that the object is weakly scattering, the internal field is approximately equal to the impinging field, and the phase shift of light crossing the object is still small [3]. For the typical refractive indices found in PDLC systems the maximum radius that can be considered using this method is still less than a small fraction of a micron ($R < 0.1\,\mu\text{m}$). Approximations are also available at the other extreme for optically large objects, such as the Anomalous Diffraction Approximation (ADA) for weakly scattering objects satisfying $kR \gg 1$ [4]. For even larger objects a geometrical optics approach might also be appropriate.

The modelling of complex structures in twisted nematic displays is often approached even more crudely. It is common to ignore the optical effects of the lateral structure entirely and model the system using a stratified media approximation. These methods, such as those developed by Jones and Berreman, treat the structure as uniform in the plane of the display with plane wave illumination. This is acceptable when modelling large pixels in many displays, where the edge effects have negligible influence. However, when modelling high performance displays, or displays with small pixels where the edge effects may be important, a more advanced method allowing for optical scattering is needed.

It is very clear therefore that the aforementioned methods fail to address accurately the light scattering from objects whose structure is on the micron scale, i.e. those which can strongly scatter light. This paper discusses numerical methods, which allows us to consider the realistic cases of PDLC structures and pixel edge structures with dimensions directly comparable to the optical wavelength ($R \cong 1\,\mu\text{m}$). As no approximations can be justified, light scattering is addressed by employing the Finite-Difference Time-Domain (FDTD) method, which is a purely numerical method for general electromagnetic field simulations. The FDTD method has been successfully used so far for studying light wave propagation through a number of liquid crystal display-type devices, including the case of twisted nematic micro-pixel devices [5,6], as well as ferroelectrics [7]. No assumptions need to be made about the relative values of the liquid crystal refractive indices. In addition, the illuminating light need not be a plane

wave, and for the PDLC modelling the more general case of Gaussian Beam illumination is demonstrated.

As this paper intends to concentrate on basic ideas, a two-dimensional approach is followed for convenience in the numerical calculations, and the results are given for the cylindrical counterparts of the most commonly encountered PDLC droplet configurations and the edges of pixels (not the corners). In particular, the radial, bipolar, axial and concentric PDLC configurations are studied and compared to the response of an identically sized isotropic cylinder. Near field data are obtained, which clearly demonstrate the inclusion in the calculations of all electromagnetic phenomena taking place. For the pixel edge an isolated pixel in a reflective structure is considered.

DESCRIPTION OF NUMERICAL TECHNIQUE

The geometry under study for the PDLC case is depicted in Figure 1. A single PDLC cylindrical object of radius R and optical dielectric tensor $\tilde{\varepsilon} = \tilde{\varepsilon}(x, z)$ is embedded in an isotropic polymer characterized by the refractive index n_{iso}. Light wave scattering will be formulated in terms of Maxwell's curl equations, which are written in the time-domain as:

$$\frac{\partial \mathbf{D}}{\partial t} = \nabla \times \mathbf{H} - \mathbf{J}_s, \tag{1a}$$

$$\frac{\partial \mathbf{H}}{\partial t} = -\frac{1}{\mu_0}\nabla \times \mathbf{E} - \frac{1}{\mu_0}\mathbf{M}_s; \quad \mathbf{D} = \tilde{\varepsilon}\mathbf{E}. \tag{1b}$$

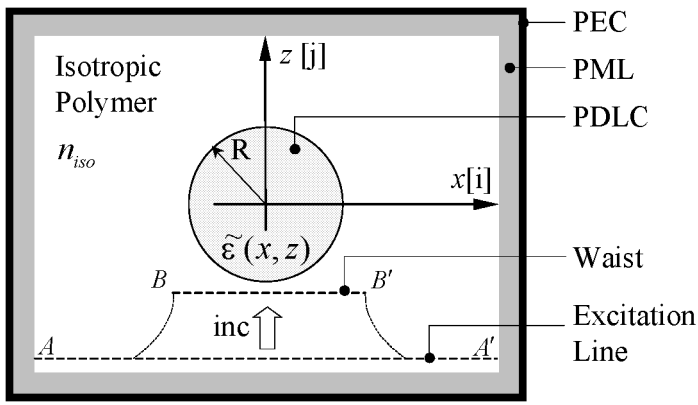

FIGURE 1 FDTD computational space arrangement for PDLC simulations with Gaussian Beam illumination. PEC = Perfect Electric Conductor, PML = Perfectly Matched Layer.

The source terms corresponding to the electric ($\mathbf{J}_s$) and magnetic ($\mathbf{M}_s$) currents will be described later on, in order to introduce the illuminating beam into the FDTD grid.

Computational space discretisation is provided by a planar variant of the original Yee cell [8]. Equations (1a) and (1b) are then time-marched using a leap-frog scheme, where dielectric displacement and electric field values are recorded at $t = n\delta t$ and magnetic field values are recorded at $t = (n + \frac{1}{2})\delta t$. Equation (1a) is first time advanced by δt and the computed displacement values are used for deducing the corresponding electric field values through $\mathbf{E} = \tilde{\varepsilon}^{-1}\mathbf{D}$, which are subsequently fed into the right hand side of Eq. (1b) in order to allow time advancement. The whole update algorithm is completely explicit, as expected.

Efficient computational space termination is provided by surrounding the scattering object by four Perfectly Matched Layer (PML) slabs, as introduced in [9]. The PML provides a theoretically reflectionless interface with the surrounding polymeric material, irrespective of the angle of incidence, and in addition provides exponential attenuation to the entering fields through its anisotropic conductivities. Field splitting is used and the usual matching conditions are employed [9]. The outer ends of the PML slabs are in contact with a Perfect Electric Conductor (PEC), as illustrated in Figure 1. In the pixel edge calculation the PML slabs at the left and right ends are replaced with periodic boundary conditions, as discussed in [7].

For the pixel edge case a simple plane wave illumination at normal incidence will be used. However, for the PDLC case an incident Gaussian beam will be considered for the illumination. In a strict sense, the Gaussian beam solution corresponds to a scalar wave equation solution under the paraxial limit. Therefore, for the two-dimensional case considered here the scalar Gaussian beam expression can be used to designate the $\hat{\mathbf{y}}$ component of the incident magnetic field if a beam polarized long the $\hat{\mathbf{x}}$ direction is to be described. For a $\hat{\mathbf{y}}$ polarized beam one can simply assign the scalar Gaussian expression to the incident $\hat{\mathbf{y}}$ component of the electric field. In the geometry used here this latter illumination does not sense the anisotropy (electric field always perpendicular to the director) and it will not be considered further. The expression for a 2-D Gaussian beam follows, which is a slight modification of the 3-D one [10]:

$$G^{inc}(x,z) = \sqrt{\frac{w_0}{w(z)}}\exp\left\{-\frac{x^2}{w^2(z)}\right\}\exp\left\{-j\frac{kx^2}{2R(z)}\right\} \times \exp\left\{-j\frac{kx^2}{2R(z)}\right\}\exp\left\{-jk(z-z_0)+\frac{1}{2}j\theta(z)\right\}, \quad (2)$$

$$w^2(z) = w_0^2\left[1 + \left(\frac{\lambda(z-z_0)}{\pi w_0^2 n_{iso}}\right)^2\right], \quad R(z) = (z-z_0)\left[1 + \left(\frac{\pi w_0^2 n_{iso}}{\lambda(z-z_0)}\right)^2\right],$$
$$\theta(z) = \tan^{-1}\left(\frac{\lambda(z-z_0)}{\pi w_0^2 n_{iso}}\right).$$

In the above equations λ is the free space wavelength, the beam waist is located at $z = z_0$, w_0 is the spot size and $k = (2\pi/\lambda)n_{iso}$. Following the above discussion the incident field components are then given by:

$$\mathbf{H}^{inc}(x,z) = G^{inc}(x,z)\hat{\mathbf{y}}, \tag{3a}$$

$$\mathbf{E}^{inc} = \frac{1}{j\omega\varepsilon_{iso}}\nabla \times \mathbf{H}^{inc}. \tag{3b}$$

The Gaussian beam will be introduced into the FDTD grid by specifying the appropriate electric and magnetic currents [11]. As propagation along the positive z direction is assumed for the incident beam, the expressions for the source currents will be given by:

$$\mathbf{J}_s = \hat{\mathbf{n}} \times \mathbf{H}^{inc}; \quad \mathbf{M}_s = -\hat{\mathbf{n}} \times \mathbf{E}^{inc}, \tag{4}$$
$$\hat{\mathbf{n}} = \hat{\mathbf{z}}.$$

It is obvious from Eq. (1a) that the electric current components should be supplied at the same grid locations as the corresponding electric field (or dielectric displacement) components in the FDTD grid. The same also applies from Eq. (1b) to the magnetic current components and the magnetic field spatial locations. For the temporal placement the electric current coincides with the magnetic field, whereas the magnetic current coincides with the electric field. Using the standard Yee cell arrangement, and taking into consideration the leapfrog scheme in time, one can develop the discrete form for the various source currents:

$$J_{s,x} = -H_y^{inc}\left(\left(i+\frac{1}{2}\right)\delta x, J_E\delta z\right)\exp\left\{j\left(n+\frac{1}{2}\right)\omega\delta t\right\}, \tag{5a}$$

$$J_{s,y} = H_x^{inc}(i\delta x, J_E\delta z)\exp\left\{j\left(n+\frac{1}{2}\right)\omega\delta t\right\}, \tag{5b}$$

$$M_{s,x} = E_y^{inc}\left(i\delta x, \left(J_E-\frac{1}{2}\right)\delta z\right)\exp\{jn\omega\delta t\}, \tag{5c}$$

$$M_{s,y} = -E_x^{inc}\left(\left(i+\frac{1}{2}\right)\delta x, \left(J_E-\frac{1}{2}\right)\delta z\right)\exp\{jn\omega\delta t\}. \tag{5d}$$

In the above equations the index J_E corresponds to the line where the excitation is introduced for the electric current components (line AA' in Figure 1), while the magnetic current components are introduced $-\delta z/2$ apart, as indicated by Eqs. (5c) and (5d). When implementing the FDTD method both time dependencies ($\cos(\omega t)$, $\sin(\omega t)$) are used to facilitate the extraction of the amplitude and phase for the various phasors involved, by employing the extractor algorithm [12,13].

APPLICATIONS

PDLC Example

As example numerical applications we will examine the scattering characteristics for the most commonly encountered PDLC configurations and a nematic pixel edge in reflection. For the PDLC case, if homeotropic anchoring conditions are met at the droplet boundary, then a stable radial configuration is predicted with a singularity in the centre. Subsequent application of an external electric or magnetic field evolves the radial configuration into an axially aligned structure. The case of parallel alignment at the droplet boundary leads to the commonly observed bipolar configuration, which is characterised by the occurrence of two singularities. Parallel alignment can also lead to a stable concentric configuration. These characteristic configurations are schematically depicted in Figure 2. For the nematic material the ordinary refractive index is $n_0 = 1.5$, the extraordinary refractive index is $n_e = 1.6$ and the surrounding polymer has a refractive index matching the ordinary one, i.e. $n_{iso} = 1.5$.

The incident light in all cases has a free space wavelength $\lambda = 633\,nm$ and propagates along the positive $\hat{\mathbf{z}}$ direction. For the PDLC, the focal plane of the beam (beam waist depicted by the line BB' in Figure 1) coincides with the centre of the computational space ($z = 0$), which is also the centre of the PDLC object. Its magnetic field vector lies along the $\hat{\mathbf{y}}$ direction resulting in non-zero electric field components along $\hat{\mathbf{x}}$ and $\hat{\mathbf{z}}$ directions. As has been explained in the previous section, the beam is introduced by specifying the appropriate electric and magnetic currents along two

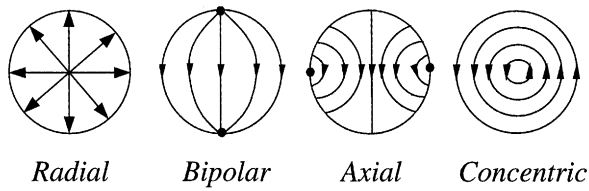

FIGURE 2 Most commonly encountered PDLC director configurations.

separate lines, just above the lower PML slab. A spot size of $w_0 = 0.5\,\mu m$ is used, corresponding to the limiting case where the scalar Gaussian beam expressions can be used for the description of the incident vector beam. If more focused beams are to be analysed, one would have to represent the incident vector beam with more accurate analytical expressions [10].

Near-field intensity maps for the total field (incident plus scattered) are given in Figure 3. For all calculations a square FDTD grid with $\delta x = \delta z = 10\,nm$ has been used to accurately resolve the object circumference ($R = 1\,\mu m$), in conjunction with a temporal step of $\delta t = 0.02\,fs$. PML slabs having a thickness of 24 Yee cells are used for space termination. Figure 3a shows the incident beam in the absence of the scattering object. Figure 3b depicts the reference case of an isotropic object with refractive index equal to the extra-ordinary refractive index $n = n_e$. Figures 3c, 3d, 3e, 3f correspond to the radial, bipolar, axial and concentric configurations, respectively. To aid the understanding of these the positioning of the PDLC object is clearly marked. The graphs lucidly demonstrate the scattering effects taking place in the near field, as described by Maxwell's equations and determined using the FDTD method.

The isotropic object having a higher refractive index compared to the surrounding medium provides focusing of the incident beam along the forward direction. The radial configuration shown in Figure 3c results in a broad scattering pattern in the forward direction, whereas the back-scattering is rather week as the nematic molecules close the beam axis are roughly aligned along the direction of propagation for the incident beam. Also the axial configuration of Figuire 5e presents a very weak scattering pattern as the two singularities are located in regions of low incident power and the rest of the structure mainly aligns along the direction of the propagating beam. As seen in Figure 3d the bipolar configuration strongly scatters light in the forward and backward directions due to presence of the two defects (singularities). The concentric configuration results in forward scattering, which is similar to that obtained in the isotropic case. This is expected as the nematic molecules close to the beam axis roughly align perpendicular to the direction of beam propagation. Therefore, the $\hat{\mathbf{x}}$ polarised incident Gaussian beam will experience the extra-ordinary refractive index, leading in a forward scattering prediction close to the isotropic counterpart. Backscattering is also quite strong due to the maximum contrast seen in the refractive indices.

Reflective Twisted Nematic Pixel-Edge Example

The director structure in the vicinity of a pixel edge in twisted nematic devices is well established and it is accurately determined by the appropriate minimisation of the elastic and electrostatic energy sum. Within the

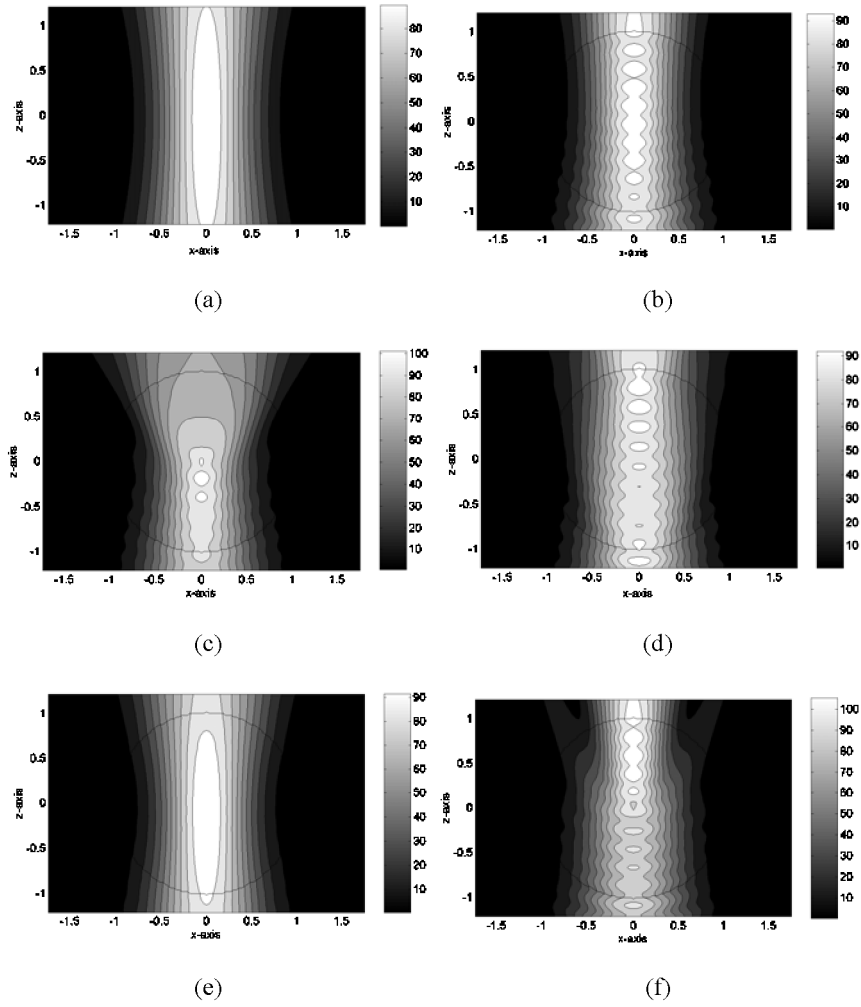

FIGURE 3 Near field intensity maps in the vicinity of the PDLC object. The illuminating Gaussian beam arrives from the lower side of the computational space, and its beam waist would have been coincident with the centre of the computational space, in the absence of the scattering object. The spot size is $w_0 = 0.5\,\mu\text{m}$. (a) Reference beam in the absence of object; (b) Isotropic object with $n_{iso} = n_e$; (c) Radial; (d) Bipolar; (e) Axial; (f) Concentric.

context of this example a pixel edge in a reflective twisted nematic device will be analysed. The structure under study is shown in Figure 4 and it corresponds to a microdisplay operating in a 63° Twist Mode with 3° of pretilt [15]. Cell thickness and birefringence are set to satisfy $d\Delta n/\lambda = 0.354$ at

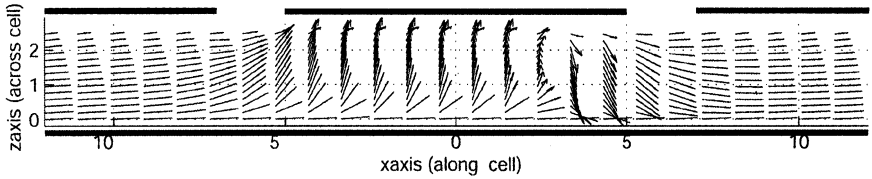

FIGURE 4 Director profile in the vicinity of pixel edges corresponding to a 63^o twist mode of operation. Cell thickness is $d = 2.65\,\mu$m and the driving voltage at the central electrode is $V = 3$ Volts. Axes are scaled in microns.

633 nm. The top patterned electrodes are made of Al and thus are reflecting, whereas the lower electrode is transparent (ITO). A voltage of 3 Volts is driving the central electrode and no voltage is applied to the left and right electrodes. It is clearly seen in Figure 4 that a strong reverse tilt disinclination line has been formed under the right edge of the central electrode, as expected.

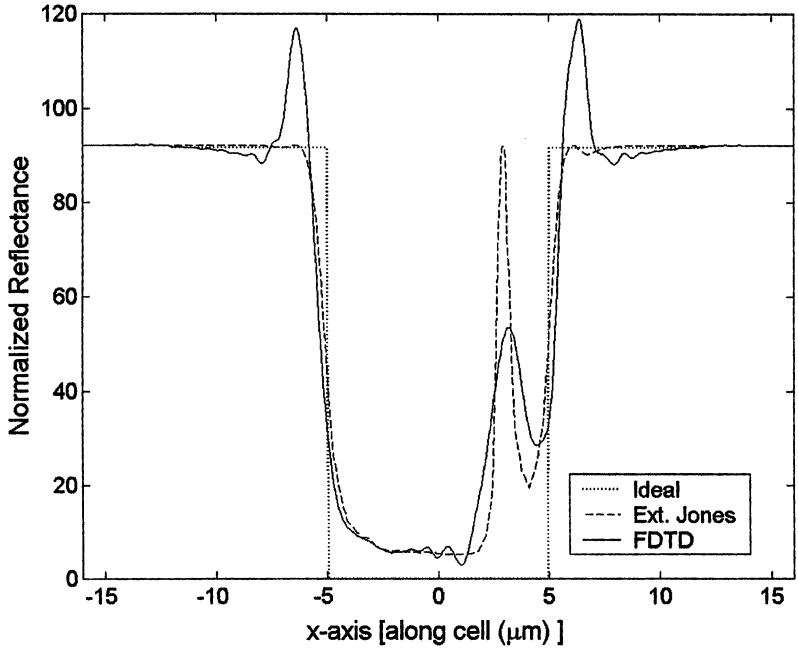

FIGURE 5 Normalised reflectance along the lower device face for the director profile shown in Figure 4. The polariser is oriented parallel to the director at $z = 0$ and it is combined with a quarter wave plate for normally white operation.

In order to produce a structure suitable for modelling an isolated switched-on pixel we used uniform extensions of the structure in the lateral ($\hat{\mathbf{x}}$) direction (resulting in a total span of 32 μm out of which only 24 μm are shown in Figure 4). This was done to remove any artefacts that might be associated with the periodic boundary conditions used for grid truncation in the lateral direction.

For normally white (NW) mode of operation a quarter wave plate is placed in the entrance (lower) face of the device after the polariser. The polariser is aligned along the entrance LC director, which coincides with the $\hat{\mathbf{x}}$ direction. Figure 5 plots the normalised reflectance along the lower device face, as calculated by the FDTD method. In the same graph a prediction obtained by the Extended Jones method is shown, by slicing the director profile into stratified columns. For reference purposes the idealised response has also been included. Figure 5 clearly demonstrates the departure from the idealised electro-optic response of the device. It also shows the difference from the less rigorous but more commonly used Extended Jones method, in particular close to the pixel edges and in the vicinity of the reverse tilt disinclination line. These effects are of physical origin and they are attributed to the strong LC director gradients taking place in these regions.

The near-field data can be used in a second stage together with an appropriate near to far field transform, in order to obtain the far field device response as perceived by the display observer.

CONCLUSIONS

The scattering properties of cylindrical PDLC objects and a pixel edge of a reflective structure have been investigated by the 2-D FDTD method. For the PDLC case a Gaussian beam incidence is implemented in conjunction with the FDTD method to simulate novel illumination conditions, where the Gaussian beam can also be thought of as the superposition of individual plane waves travelling in different directions. Calculations are focused on the most demanding case of practical PDLC structures with dimensions directly comparable to the optical wavelength ($R \cong 1\,\mu\text{m}$), where no approximations can be justified. Simulated results correspond to a strict numerical solution of Maxwell's equations.

REFERENCES

[1] Crawford, G. P. & Zumer, S. (1996). *Liquid Crystals in Complex Geometries*, Taylor & Francis, London.

[2] Collings, P. J. & Patel, J. S. (1997). *Handbook of Liquid Crystal Research*, Oxford University Press, New York.

[3] Zumer, S. & Doane, J. W. (1986). *Phy. Rev. A*, *34*, 3373.
[4] van de Hulst, H. C., (1957). *Light Scattering by Small Particles*, Dover: New York.
[5] Witzigmann, B., Regli, P., & Fichtner, W. (1998). *J. Opt. Soc. Am. A.*, *15*, 753.
[6] Kriezis, E. E. & Elston, S. J. (2000). *Optics Comm.*, *177*, 69.
[7] Kriezis, E. E., Filippov, S. K., & Elston, S. J. (2000). *J. Opt. A: Pure Appl. Opt*, *2*, 27.
[8] Yee, K. S. (1966). *IEEE Trans. Antennas Propag., 14*, 302.
[9] Berenger, J. P. (1994). *J. Comp. Phys.*, *114*, 185.
[10] Varga, P. & Torok, P. (1998). *Optics Comm.*, *152*, 108.
[11] He, Y., Kojima, T., Uno, T., & Adachi, S. (1998). *IEICE Trans. Electron.*, *E81-C*, 1881.
[12] Harms, P., Mittra, R., & Ko, W. (1994). *IEEE Trans. Antennas Propag., 42*, 1317.
[13] Ishimaru, A. (1991). *Electromagnetic Wave Propagation, Radiation, and Scattering*, Prentice Hall, New Jersey.
[14] Taflove, A. (1995). *Computational Electrodynamics: The Finite-Difference Time-Domain Method*, Artech House, Boston.
[15] Yang, K. H. & Lu, M. (1999). *Displays*, *20*, 211.